ELSEVIER

Journal of Power Sources 113 (2003) 19–36

JOURNAL OF POWER SOURCES

www.elsevier.com/locate/jpowsour

Catalytic burner for an indirect methanol fuel cell vehicle fuel processor

Meenakshi Sundaresan[a,*], Sitaram Ramaswamy[a], Robert M. Moore[a], Myron A. Hoffman[b]

[a]*Institute of Transportation Studies, University of California-Davis, Davis, CA 95616, USA*
[b]*Mechanical and Aeronautical Engineering Department, University of California-Davis, Davis, CA 95616, USA*

Received 22 August 2002; accepted 2 September 2002

Abstract

Major impediments to the wide-scale implementation of hydrogen/air fuel cell vehicles are the lack of hydrogen infrastructure and on-board hydrogen storage. One proposed source of hydrogen exists in the development of on-board methanol (and other hydrocarbon) fuel processors. Packaging limitations and fuel processor performance constraints on efficiency and transient response play key roles in vehicular applications. These constraints may be addressed by considering proper thermal integration between two major components of the fuel processor: the reformer and catalytic burner.

The focus of this research is on the effects of the catalytic burner on reformer performance in a thermally well-integrated configuration. Specifically, the work has focused on the generation of a detailed numerical model incorporating kinetics and mass and heat transfer to accurately characterize the burner. Unlike a simple, thermodynamic model, the detailed model provides a level of complexity necessary to understand the impact of thermal integration on reformer transient response, reformate composition, and emissions.

Keywords: Indirect methanol fuel cell vehicle; Reformer; Burner; Thermal integration; Transient response

1. Introduction

Hydrogen/air fuel cell vehicles are currently receiving much attention as an alternative to internal combustion engine vehicles (ICEVs) because of their potential to reduce fuel consumption and emissions. However, the combined problems of on-board hydrogen storage and the lack of hydrogen infrastructure represent major impediments to their wide-scale adoption as replacements for ICEVs. On-board fuel processors that generate hydrogen from on-board liquid methanol (and other hydrocarbons) have been proposed as alternative hydrogen sources for the fuel cell. The indirect methanol fuel cell vehicle fuel processor uses steam reformation of methanol to produce hydrogen required by the fuel cell. Since steam reformation is an endothermic process, a heat source, such as a catalytic burner, is required to supply the necessary thermal energy.

Packaging limitations and fuel processor performance constraints such as high efficiency and fast transient response play key roles in vehicular applications. Components within the fuel cell system have transient response times on the order of milliseconds; however, the fuel processor can take on the order of several seconds for transient response. These constraints may be addressed by considering proper thermal integration between the reformer and burner.

Several configurations of the burner and reformer have been proposed and have been published in the literature [1–3] such as shell-and-tube heat exchanger and concentric burner and reformer arrangements. However, these configurations have limitations in terms of transient response. Results of one modeling study [1] of a dynamic reformer sized to produce hydrogen for an 80 kWe PEM fuel cell stack show ramp down response greater than 10 s to reach steady state. The configuration considered is a series of tubes filled with copper and zinc oxide catalyst surrounded by tube walls and hot gas. Similarly, in another study [2], a tubular reactor was modeled that generates hydrogen required for a 400 kWe PEM fuel cell stack. The heat is transferred to the inner wall of the reformer from a concentric heat source. Results suggest that response times on the order of 15–20 s are possible. Finally, an experiment was conducted on a fuel

* Corresponding author. Tel.: +1-530-792-1033; fax: +1-530-752-6572.
E-mail address: msundaresan@ucdavis.edu (M. Sundaresan).

0378-7753/02/$ – see front matter
PII: S0378-7753(02)00478-0

Nomenclature

Unless indicated otherwise, the following nomenclature applies to the equations presented in this paper. Note that "catalyst" implies catalyst plus the catalyst support system.

A	reaction surface area in one CSTR, (m^2; product of S_{cat}, A_c, ξ, Δx)
A_c	reactor cross-sectional area (m^2)
C or [ ]	concentration (mol/m^3)
C_p	specific heat (J/mol K)
$C_{p_{cat}}$	catalyst specific heat (J/kg K)
$C_{p_{wall}}$	wall specific heat (J/g K)
F or dn/dt or $\dot{n}$	flowrate (mol/s)
h	enthalpy (J/mol)
h_D	mass transfer coefficient (m/s)
h_t	heat transfer coefficient (W/m^2 K)
S	open frontal area fraction
S_{cat}	1-S

Methanol reaction

k_1	gas reaction rate constant (s^{-1})
k_2	surface reaction rate constant (m/s)

Nitric oxide (NO) reaction

k_1, k_2	reaction rate constants (m^3/(mol s))
m_{cat}	catalyst mass (kg)
m_{wall}	wall mass (g)
n	specie quantity (mol)
r	reaction rate (mol/s)
$\bar{R}$	universal gas constant (8.315 J/mol K)
P	pressure (Pa)
$\dot{Q}_{reformer}$	reformer heat rate requirement (J/s)
T	temperature (K)
UA	product of heat transfer coefficient and area (W/K)
$U_{burner-wall-side}A_{wall}$	product of the heat transfer coefficient between the burner catalyst and wall and wall area
$U_{reformer-wall-side}A_{wall}$	product of the heat transfer coefficient between the wall and reformer catalyst and wall area
V_{void}	void volume of one CSTR, (m^3; product of S, A_c, Δx)

Greek symbols

Δx	length of one CSTR (m)
λ	thermal conductivity (W/m K)
ρ_{ca}	catalyst density (kg/m^3)
ξ	specific surface area (m^2/m^3 bed volume (bed volume = catalyst + void))

Subscripts

i	ith specie
g	gas
cat	catalyst
T	total
in	entrance

processor system in which catalytic burners were placed in an annular arrangement at the bottom of a 50 kW (H_2) compact reformer [3]. Transient response times were measured to be about 20 s.

Some organizations are working toward improving transient response times by experimenting with and modeling the plate configuration [4–6], typically in which one side of a plate is covered with reformer catalyst and the other side is covered with combustion catalyst. All of these groups studied units that could produce hydrogen for a 20 kWe fuel cell stack. One study [4] integrated reforming, combustion and selective oxidation (used to oxidize the CO in the reformate which can otherwise poison the fuel cell) catalysts coated onto aluminum substrates in a prototype unit. The heat transfer characteristics of the compact heat exchange units could satisfy transient response requirements for which the goal was set at less than 5 s.

The literature presents examples of on-going experimental and modeling efforts in characterizing a thermally well-integrated system. While studies have been conducted on the effects of a thermally well-integrated system on reformer performance under steady state conditions, this paper provides simulation results of a detailed model run under varying and dynamic conditions. The model was developed using Matlab/Simulink software. The results of research discussed in this paper are based on this model, which is part of a fuel cell system designed for integration into a larger indirect methanol fuel cell vehicle model.

This paper is comprised of two major sections: (1) a description of the steps taken in generating a detailed model that will accurately characterize a thermally integrated burner/reformer system, and (2) a description of simulation results that show the effects of thermal integration on: (a) reformer temperature and emissions especially when varying spatial parameters such as catalyst loading, (b) sensitivity to changes in input flow or thermal mass, (c) dynamic response, and (d) burner emissions. Vehicle startup and control issues and discussion of a detailed reformer model are not part of this paper. A paper on the detailed reformer model is forthcoming.

2. Background of the detailed model

2.1. Indirect methanol fuel cell (IMFC) system

The burner is part of the fuel processor that is part of a larger fuel cell system. As shown in Fig. 1, the burner

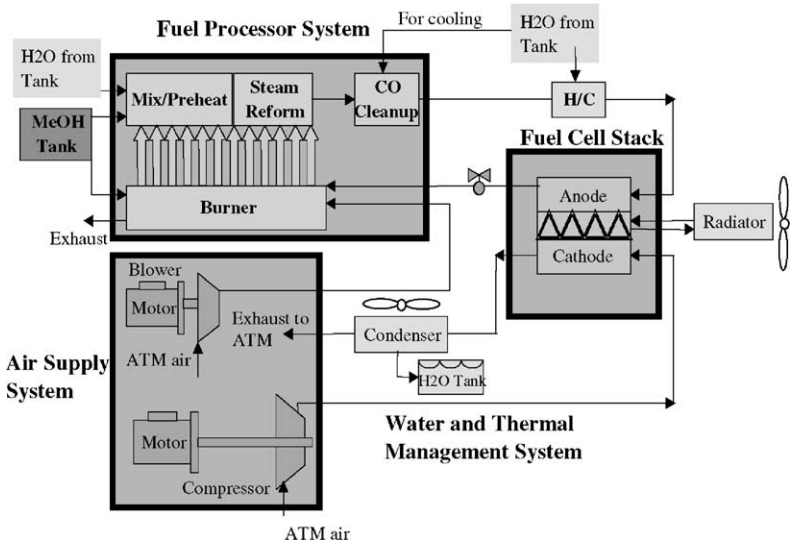

Fig. 1. Schematic of the IMFC system as studied in the IMFC vehicle model.

receives methanol from an on-board tank, air from a blower and, in some operating conditions, exhaust from the fuel cell anode, which consists of hydrogen, CO_2 and water vapor. The burner provides heat to a preheater and the steam reformer.

Typically, the burner, via an intermediate heat transfer medium, heats the reformer. In the simplest shell and tube model, the burner hot gases provide the energy needed to heat the reformer. As high temperatures are not desired due to NO_x formation and gases have low heat capacity, the flowrate of the gases must be very high to ensure adequate heat transfer to the reformer. High temperatures and flowrates are not desirable operating conditions, and alternate methods such as hot oil as an intermediate thermal medium have been used in some cases. This method has its own drawbacks since hot oil would introduce additional thermal mass that would need to be heated. Due to the limitations of conventional approaches, a survey of existing on-going industrial efforts in this area indicates that well-integrated burner/reformer designs are currently being pursued by a number of different organizations [4–6]. One abstracted physical representation of such a model is as shown in Fig. 2.

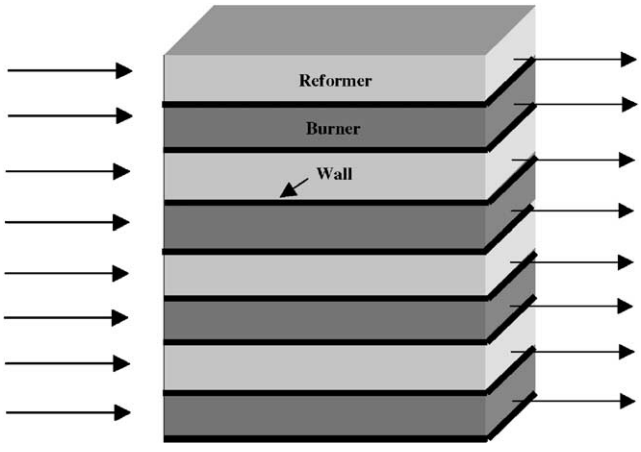

Fig. 2. Physical representation of thermally integrated burner and reformer bi-catalyst plate configuration.

One side of each plate is coated with the reformer catalyst and the other side with the burner catalyst. This burner/reformer configuration uses conduction across the width of a thin plate as a mode of heat transfer from the burner to the reformer. This results in very rapid transfer of heat from the burner to the reformer compared to some alternate methods. Even though improvements in other burner/reformer configurations continue, the plate design is chosen as the physical burner/reformer model in this paper.

2.2. Mathematical modeling

In the process of developing the model, the level of detail had to be assessed. A simple, thermodynamic model with inlet and exit states would provide only such information as adiabatic temperature and exit composition at equilibrium. However, there are some reasons why a more detailed model is required. First, within the fuel cell system the fuel processor has a slow transient response relative to the other components and it cannot be assumed that thermal equilibrium is reached for every input flow change. Only a chemical kinetic model can determine the instantaneous output conditions for a dynamic input. Second, as the burner and reformer are thermally integrated, the instantaneous burner conditions directly affect the reformer conditions. Finally, the literature provided sources of kinetic data which could be used to validate the model against laboratory results. Developing a detailed model allowed a level of accuracy to be ascertained.

Once it was determined that a kinetic model should be used, the modeling technique had to be established. For the catalytic burner, a plug flow reactor configuration

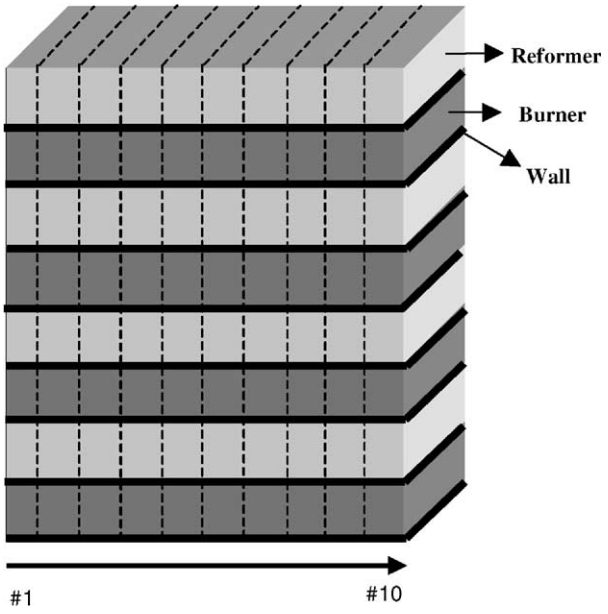

Fig. 3. Ten CSTR discretization of plate configuration.

represented by a series of continuously stirred tank reactors (CSTRs) was assumed. Ideally, a plug flow reactor has no mixing of the flow in the axial direction and perfect mixing in the radial direction. Concentration and temperature gradients occur in the axial direction only. Each CSTR, however, has perfect mixing such that the reactor contents are spatially uniform. The modeling methodology is to discretize the reactor into several elements in the axial direction, and assume all the quantities to be uniform in each element in a finite difference approximation of spatial gradients. The number of elements is dictated by the balance between accuracy and computational complexity. Since the reformer model was also constructed using the CSTR approach and the burner was integrated with the reformer, it was determined that 10 CSTRs would be used based on a literature search conducted for the reformer [2,7]. To relate the plate configuration to the 10 CSTR modeling methodology, Fig. 3 is shown with lines to illustrate discretization.

2.3. Burner kinetics

The plug flow configuration for the burner was modeled based on the experimental and numerical work done by [8]. The burner kinetics are based on a platinum-loaded gamma alumina monolith reactor and assume oxidation of methanol in a one-step reaction. Fig. 4 illustrates a representation of a monolith channel where reactions take place in the gas and on the catalyst particles which are washcoated onto the substrate surface. The open frontal area, which is the porosity, void, or free cross-sectional area available for flow, is 64%. It was determined in the present analysis that a total reactor volume of 0.0041 m^3 is required to ensure complete conversion of the methanol.

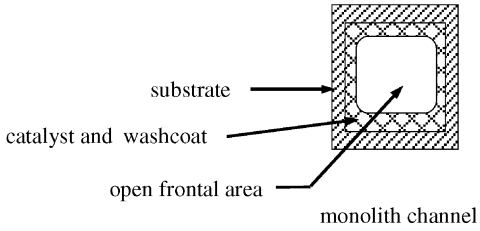

Fig. 4. Schematic representation of a monolith channel (not to scale).

The reactor is assumed to operate at atmospheric pressure, the gas mixture is an ideal gas, and pressure drop is neglected.

2.3.1. Rate expressions used

Rate expressions are provided in [8] for the gas and surface reaction, where the reaction rate constants (k_1 and k_2, described below) were experimentally determined and one-step Arrhenius rate expressions for complete oxidation reactions for the surface and gas were developed. Based on the earlier work of [8] of methanol oxidation on platinum, it was determined that the reaction order of methanol was first-order and oxygen was zero-order. The methanol reaction rates were determined under steady state conditions by the difference between the methanol concentration at the inlet and the outlet of the experimental catalytic reactor. The methanol oxidation equation is shown in Eq. (1).

$$CH_3OH + \tfrac{3}{2}O_2 = CO_2 + 2H_2O \quad (1)$$

The homogeneous reaction rate of methanol is shown in Eq. (2).

$$r_{CH_3OH} = k_1 C_{CH_3OH_g} V_{void} \quad (2)$$

$C_{CH_3OH_g}$ is the concentration of methanol in the gas, reaction rate constant $k_1 = e^{(-6.1\times10^3/(\bar{R}T_{burner})+3.2)}$, and V_{void} is the burner void volume for one CSTR, which is calculated using the open frontal area.

As shown in Eq. (3) the concentration of surface methanol, $C_{CH_3OH_{cat}}$, had to be determined by equating two surface reaction rate expressions:

$$r_{CH_3OH} = h_D(C_{CH_3OH_g} - C_{CH_3OH_{cat}})A,$$
$$r_{CH_3OH} = k_2 C_{CH_3OH_{cat}} A \quad (3)$$

Solving for $C_{CH_3OH_{cat}}$ yields the following expression:

$$C_{CH_3OH_{cat}} = \frac{C_{CH_3OH_g} h_D}{k_2 + h_D}$$

The term h_D is the mass transfer coefficient, the reaction rate constant $k_2 = e^{(-5.9\times10^4/(\bar{R}T_{burner})+22.45)}$ when $T_{burner} < 380$ K and $k_2 = e^{(-6.4\times10^3/(\bar{R}T_{burner})+5.8)}$ when $380\ K \le T_{burner} < 830$ K, and A is the reaction surface area. The reaction rates of the other species in the methanol reaction are based on Eqs. (2) and (3) and the reaction stoichiometry. The mass transfer coefficient, h_D, is 0.235 m/s and was determined from [9].

Energy and species balance calculations are performed in each CSTR. Eqs. (4)–(8) are used in the species balance.

$$\frac{dn_{i_{cat}}}{dt} = -r_{i_{cat}} \quad (4)$$

The term $dn_{i_{cat}}/dt$ is the flowrate due to reactions and $r_{i_{cat}}$ the reaction rate, both for the ith surface specie. Note the sign convention for reaction rates as used in the model.

$$\frac{dn_{i_g}}{dt} = F_{i(in)} - (r_{i_g} + r_{i_{cat}}) - F_i \quad (5)$$

The term dn_{i_g}/dt is the flowrate due to reactions and flows into and out of the burner, r_{i_g} the reaction rate, $F_{i(in)}$ the flowrate into the burner and F_i the flowrate out of the burner, all for the ith gas specie.

$$n_T = \frac{PV_{void}}{\bar{R}T_{burner}} \quad (6)$$

The term n_T is the total moles, assuming ideal gas conditions, P the burner total pressure, T_{burner} the burner temperature, and $\bar{R}$ the universal gas constant. Note that calculations are done with moles and therefore use the universal gas constant $\bar{R}$; however, while moles are not conserved, mass is conserved. This condition was verified within the model. The initial conditions for moles are $n_{O_2} = 0.2n_T$, and $n_{N_2} = 0.8n_T$ assuming only air exists within the burner at $t = 0$.

$$F_i = \frac{n_i F_T}{n_T} \quad (7)$$

The term n_i is the moles for the ith specie and F_T is the total flowrate which is further defined in Eq. (8). The initial condition for T_{burner} is 550 K.

$$F_T = \sum F_{i(in)} - \sum (r_{i_g} + r_{i_{cat}}) + \frac{PV_{void}}{\bar{R}T_{burner}^2}\frac{dT_{burner}}{dt} \quad (8)$$

The terms included in the energy balance equations depend on the level of required complexity to accurately and realistically model the burner. Two plug flow models were examined: (1) a heterogeneous model, which includes heat transfer between the surface and gas and conduction in the substrate along the burner, i.e. surface and gas temperatures are different and (2) a pseudo-homogeneous model, which assumes that the gas and surface are at the same temperature. In both cases, radiation within the combustor and to the surroundings is neglected. In the thermally integrated case, temperatures are lower than 1000 K. In combustors where temperatures are above 1000 K and can reach 1500 K, [10] recommends that heat transfer by radiation be considered. Heat loss from the combustor is assumed only to the reformer and not to the ambient environment.

Simulations were run to compare the results of the heterogeneous and pseudo-homogeneous model to determine the importance of these energy balance differences. In a full vehicle model, detailed components models such as for the heterogeneous burner would require hours of computation time, so the comparison was necessary to determine whether a simpler model such as the pseudo-homogeneous model could be used. The results of the comparison and the energy and species balance equations are provided in the next section.

2.4. Thermal coupling

The method used to thermally couple the burner and reformer CSTRs lies in linking the energy balance equations. Since heat transfers from the burner catalyst to the wall and the wall to the reformer catalyst, energy balance equations were required for the three sections. However, it was necessary to determine the importance of heat transfer between the surface and gas and conduction in the substrate along the burner, which are modes present in the heterogeneous burner configuration. Such a model would account for a difference in surface and gas temperatures; however, the pseudo-homogeneous model assumes the surface and gas temperatures are the same. As shown in the following figures, the comparison between the heterogeneous and pseudo-homogeneous models reveals little difference, especially in the reformer exit hydrogen, which is the key parameter in question. Note that the results of validation runs for the heterogeneous model compared to results of [8] are shown in Appendix A. Also note that a paper on the detailed *reformer* model is forthcoming.

Fig. 5 shows a comparison of reformer exit hydrogen for the two burner models.

The simulations were run with a methanol input flowrate stepped up to 0.35 mol/s for the reformer (and input steam at a steam/methanol ratio of 1.3) and 0.05 mol/s for the burner (and input air at a relative air/fuel ratio of 1.5). These flowrates represent one particular operating condition for the fuel processor. For reference, the reaction for the endothermic steam reformation of methanol is shown in Eq. (9). Results show only 1% difference in reformer exit hydrogen, which is considered negligible.

$$CH_3OH + H_2O = CO_2 + 3H_2 \quad (9)$$

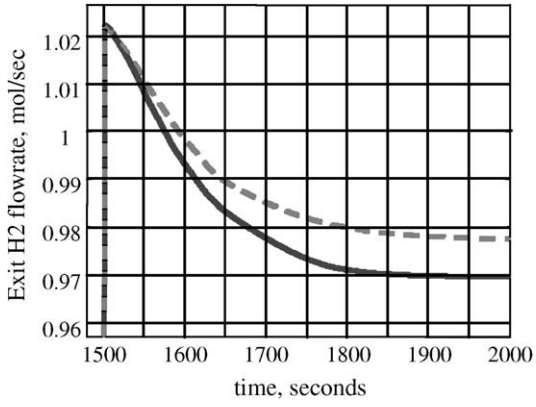

Fig. 5. Comparison of reformer exit hydrogen. (– – –) Pseudo-homogeneous model; (—) heterogeneous model. Note scaling; see Fig. 6 for full step response.

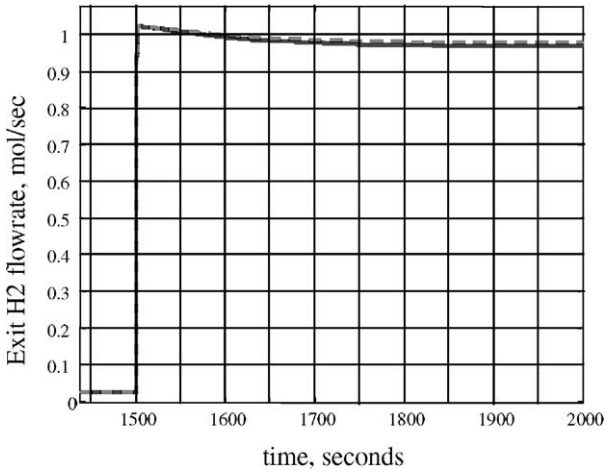

Fig. 6. Step response of exit hydrogen. (– – –) Pseudo-homogeneous model; (—) heterogeneous model.

An explanation of the transient response follows. In Fig. 6 the step occurs at 1500 s and there is the appearance of an instantaneous response.

The reason for this behavior is because the reformer has a finite volume and the latter half of the fuel processor is rich in hydrogen. When the step input of methanol/water mixture comes into the reformer, it effectively pushes the hydrogen-rich reformate out of the reformer (note that the reformer is operated in a constant pressure mode). However, this scenario cannot be sustained and the response follows first-order behavior until it approaches steady state.

Based on the comparison results, it was decided to use the simpler, pseudo-homogeneous energy balance as shown in Eq. (10). The main parameter used in the models to thermally couple the burner and reformer is UA, where U is the heat transfer coefficient and A is the area. Specifically, UA is the product of the heat transfer coefficient between the burner catalyst and wall and wall area ($U_{\text{burner–wall–side}}A_{\text{wall}}$) and the product of the heat transfer coefficient between the wall and reformer catalyst and wall area ($U_{\text{reformer–wall–side}}A_{\text{wall}}$). The "thermal coupling" is made as follows: T_{burner}, or the burner temperature in Eq. (10) is calculated and used in the wall energy balance in Eq. (11). T_{wall}, or the wall temperature in Eq. (11) is calculated and used in the heat transfer term of Eq. (12). The heat transfer term in Eq. (12) equals the heat the burner must provide and is used for the term $\dot{Q}_{\text{reformer}}$ in Eq. (10). Note that "catalyst" implies catalyst plus the catalyst support system.

$$\dot{E}_{\text{stored}} = \dot{E}_{\text{in}} - \dot{E}_{\text{out}}$$

$$\left(m_{\text{cat}}C_{\text{p}_{\text{cat}}} + \sum n_i C_{\text{p}_i}\right)\frac{\text{d}T_{\text{burner}}}{\text{d}t} = \sum F_{i(\text{in})}h_{i(\text{in})} - \dot{Q}_{\text{reformer}} - \sum\left(F_i + \frac{dn_i}{dt}\right)h_i \quad (10)$$

$$m_{\text{wall}}C_{\text{p}_{\text{wall}}}\frac{\text{d}T_{\text{wall}}}{\text{d}t} = U_{\text{burner–wall–side}}A_{\text{wall}}(T_{\text{burner}} - T_{\text{wall}}) \quad (11)$$

$$(m_{\text{cat}}C_{\text{p}_{\text{cat}}} + \sum n_i C_{\text{p}_i})\frac{\text{d}T_{\text{ref}}}{\text{d}t} = \sum(F_{i(\text{in})}h_{i(\text{in})}) + U_{\text{reformer–wall–side}}A_{\text{wall}}(T_{\text{wall}} - T_{\text{ref}}) - \sum\left(F_i + \frac{\text{d}n_i}{\text{d}t}\right)h_i \quad (12)$$

The initial condition for the temperatures are $T_{\text{burner}} = T_{\text{wall}} = T_{\text{ref}} = 550$ K, where the burner, wall and reformer are assumed to be fully warmed up at time $t = 0$. A representation of the thermal coupling between the 10 CSTRs of the reformer and burner is illustrated in Fig. 7.

$U_{\text{burner–wall–side}}A_{\text{wall}}$ and $U_{\text{reformer–wall–side}}A_{\text{wall}}$ had to be determined. However, it soon became apparent that the fuel processor would need to be scalable using the UA parameters while maintaining the validity of using the existing kinetic data.

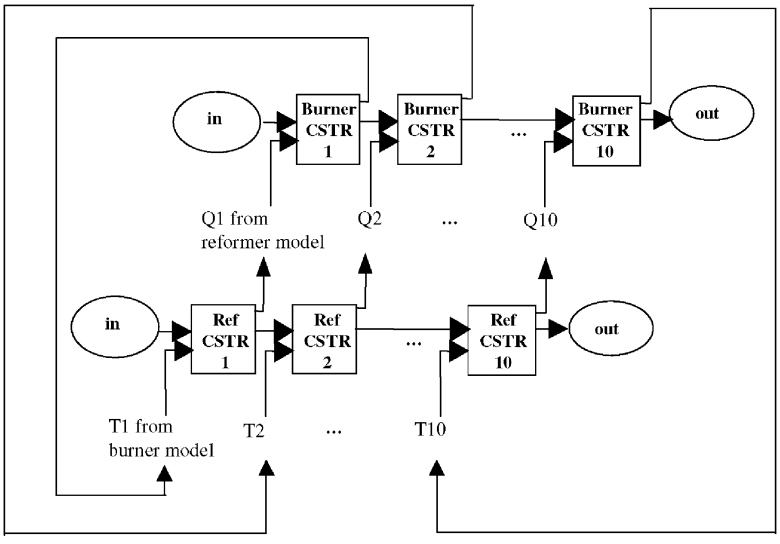

Fig. 7. Illustration of thermal coupling.

2.5. Scaling

Since kinetic expressions are non-linear, scaling a tubular reactor is not a linear process. For example, if an increase in output flowrate of X times is required, increasing reactor size either by catalyst mass or volume by X times would decrease the time it takes to get to the final product, but not increase the amount of the final product. Reaction rates are typically per unit catalyst mass or volume, so increasing either catalyst mass or volume simply increases the rate at which a reactant is consumed or product is formed. Fig. 8 illustrates three plots of response time.

Plot (a) represents the response of a 25 kg reformer, used as a baseline. Plot (b1) represents the response of a 35 kg reformer. Increasing the catalyst mass allows the reaction to proceed more quickly to the same steady state exit flow. However, as seen in plot (b2), which also represents the response of a 35 kg reformer, increased catalyst mass can take more time to reach steady state if thermal energy is inadequate.

Increasing the flowrate by X times, without an increase in catalyst mass or volume, would result in lower conversion. Fig. 9 shows the effect of increasing input flow on the same reactor. Plots (a) and (b) represent flowrates of 0.05 and 0.5 mol/s, respectively. The exit conversion is lower for the higher input flowrate.

The plate configuration is effectively having several reactors in parallel; therefore, scaling is possible by increasing the number of plates as shown in Fig. 10. Based on the maximum required exit hydrogen, one could manifold an input flowstream to the correct number of plate channels such that individual channel flows do not exceed the maximum reactant flow that still achieves the desired conversion given the reaction kinetics. It is assumed that the plates are fully warmed up. Furthermore, it is assumed that all plates are in use during system operation. Even if some plates are warm but not in use, i.e. no flow in the plate channels

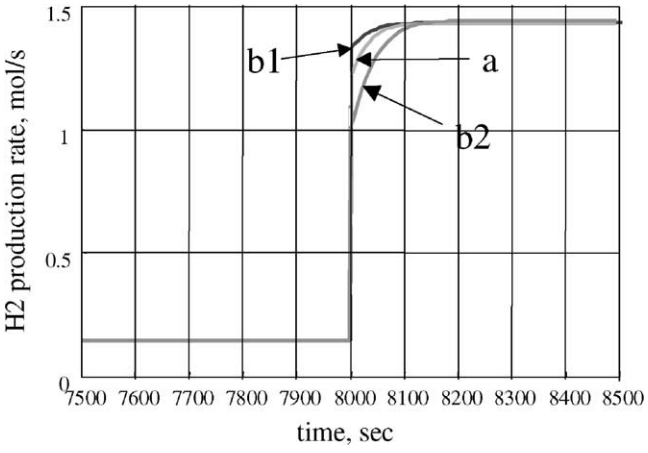

Fig. 8. Effect of increasing catalyst mass on response time: (a) 25 kg, baseline, (b1) 35 kg, faster thermal response than baseline, (b2) 35 kg, slower thermal response than baseline.

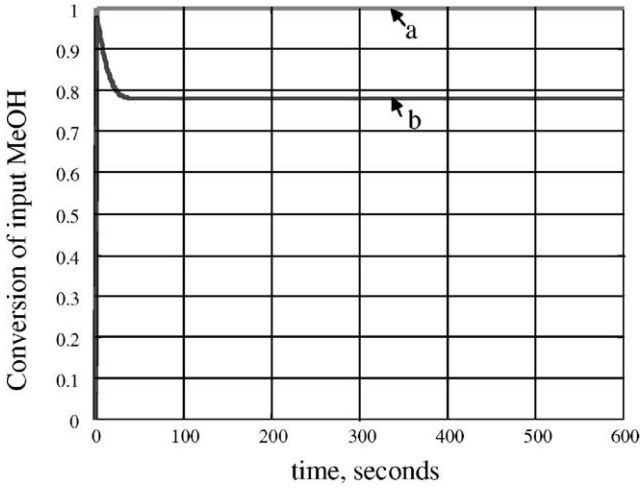

Fig. 9. Effect of flowrate on conversion: (a) 0.05 mol/s, >99% conversion, (b) 0.5 mol/s, ~78% conversion.

because full power operation is not yet needed, the response may be different than if all plate channels had a uniform, lower flowrate before being brought up to full power.

While the purpose of constructing and using this model is not to design systems, as this is dependent on vehicle design, it is important to be realistic in model parameters and make a "best-guess" assessment of packaging considerations. To make scaling in the model parameters flexible and realistic for the plate configuration, it was required that the UA parameters become independent of individual plate area. The best way to determine these UA values would be from microscale experiments. It might also be possible to estimate UA from geometrical and thermal properties or alternatively, given a value for UA, the correct set of thermal properties can lead to initial geometry estimates.

In the initial part of the analysis, the values for UA were selected using the work done earlier by [7]. That study on a shell and tube reformer/burner configuration illustrated the need for substantially higher heat transfer coefficients to achieve exit H_2 response, from 10 to 90%, of the order of 2 s,

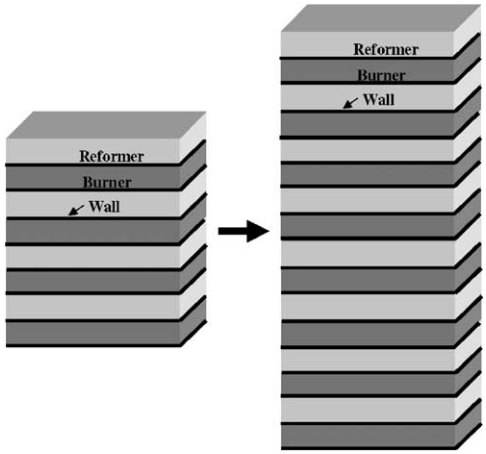

Fig. 10. Scalability with plate configuration.

which is the response time required by the fuel cell system specifications used [11]. Therefore, the initial studies of the thermally integrated reformer/burner system were based on an assumption of setting both $U_{\text{burner–wall–side}}A_{\text{wall}}$ and $U_{\text{reformer–wall–side}}A_{\text{wall}}$ equal to 60 W/K per plate (for 100 plates), which is an order of magnitude higher than the values studied by [7]. A more detailed discussion of the *UA* parameters can be found in Appendix B.

3. Model studies and results—thermal integration effects

As mentioned earlier, some advantages of the discretization of the reformer and burner into ten elements include the ability to see the effects of parametric changes and obtain local values at every point along the reactor. Discretization allows for thermally integrating the burner and reformer and varying parameters to observe the interaction between the two components. For example, variations have been studied for the burner catalyst loading and wall thermal mass. A four-section discussion describes simulation results that show the effects of thermal integration on: (a) reformer temperature and emissions especially when varying spatial parameters such as catalyst loading (Section 3.1), (b) sensitivity to changes in input flow or thermal mass (Section 3.2), (c) dynamic response (Section 3.3), and (d) burner emissions (Section 3.4). Note that despite the model's ability to accept anode exhaust as shown in Fig. 1, simulation results in this section are based on methanol input alone to observe the effects of thermal integration and eliminate the complexity of an additional fuel.

3.1. Catalyst loading

Varying the burner catalyst loading plays an important role in reducing reformer steady state temperature and carbon monoxide output. Reducing reformer temperature protects the catalyst from operating in a region in which it can deactivate due to sintering. The reformer CO formation is a strong function of temperature based on the reformer kinetic model used [12]. Reducing the reformer temperature corresponds to a reduced amount of CO.

Carbon monoxide can be a significant problem from the viewpoint of the fuel cell stack. Even while there is a CO cleanup system in place, minimizing or eliminating CO from the reformer would be an ideal condition. Modifying parameters within the reformer to control or optimize CO output would need to be considered, and as described below, these modifications can yield favorable results.

3.1.1. Simulation setup

Close thermal integration results in different responses to different types of burner catalyst loading. Three configurations along the burner are discussed and are shown in Fig. 11: (a) uniform loading, (b) gradually increasing loading, and (c) high concentration of catalyst in the second half of the burner. In all cases there is the same total amount of catalyst. Note that the *reformer* catalyst loading is uniform in this analysis. The following parameters were analyzed: (1) burner temperature, (2) reformer temperature, (3) reformer CO flow, and (4) reformer output H_2.

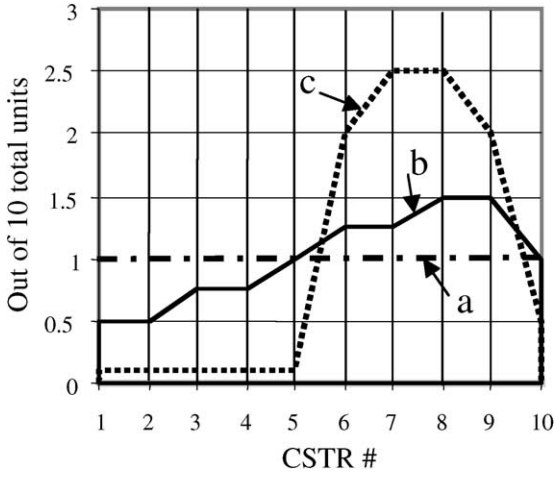

Fig. 11. Three catalyst loading distribution schemes along burner: (a) uniform, (b) gradually increasing, (c) high concentration—second half of burner.

3.1.2. Simulation results

Figs. 12 and 13 show the effects of the three catalyst loading scenarios on the burner and reformer temperature profiles. Configuration (a) represents the uniform loading scenario which has the highest temperature profile. Configuration (b) is the gradually increasing loading scenario for which the temperature in the initial CSTRs is slightly lower. For configuration (c), the temperature hovers around 550 K with the exception of the jump from the fifth to the sixth CSTR at which point the amount of burner catalyst increases, increasing the local reaction temperature.

The reformer CO formation is a strong function of temperature and this relationship is reflected in Fig. 14 which shows lower steady state molar flowrates of CO for configurations (b) and (c).

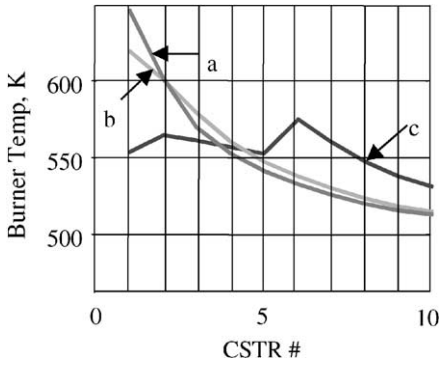

Fig. 12. Burner temperature for varied catalyst loading: (a) uniform, (b) gradually increasing, (c) high concentration—second half of burner.

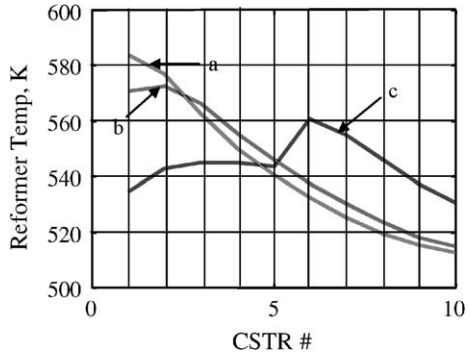

Fig. 13. Reformer temperature for varied catalyst loading: (a) uniform, (b) gradually increasing, (c) high concentration—second half of burner.

In Fig. 14, while the CO flowrate in configuration (c) appears to continue to increase at the end of the reformer, Fig. 15 shows that the output H_2 ceases to change at the end of the reformer and illustrates how the same output hydrogen in configurations (a) and (b) could be achieved with the lower CO penalty of configuration (c).

While many catalyst distributions may not have an impact or may even have an adverse impact on reformer performance, the results for the example loading schemes used in this analysis show that varied catalyst loading could play a role in decreasing reformer temperature and CO emissions.

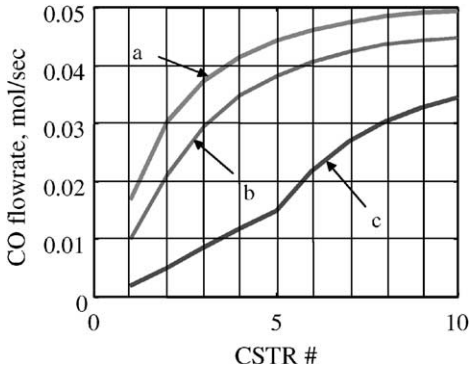

Fig. 14. Reformer CO output for varied catalyst loading: (a) uniform, (b) gradually increasing, c) high concentration—second half of burner.

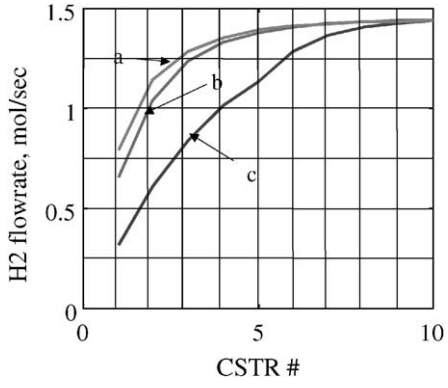

Fig. 15. Reformer H_2 output for varied catalyst loading: (a) uniform, (b) gradually increasing, (c) high concentration—second half of burner.

3.2. Sensitivities

Thermal integration makes the system more sensitive to perturbations in the input flow stream. The current model assumes no time lag between the methanol sent into the reformer and the methanol sent into the burner to generate the necessary heat for the reformer reactions to occur. However, a time lag between these flows can affect the temperature distribution of the thermally integrated components, possibly jeopardizing reformer catalyst integrity, decreasing methanol conversion and increasing carbon monoxide production. In this section, different scenarios of thermal integration are presented. At the same time, the impact of a lag on a thermally integrated system is investigated.

3.2.1. Impact of thermal integration on reformer and impact of lag on thermal integration

Based on the fuel cell stack H_2 requirement, the controller will send the required amount of methanol to the reformer and based on the heat requirement of the reformer, the controller will send the required amount of methanol to the burner. However, some drawbacks exist, including possible reformer catalyst sintering due to a higher reformer temperature as a result of the thermal integration. Furthermore, the increase in reformer temperature accelerates the production of carbon monoxide under certain transient conditions since the reformer CO formation is a strong function of temperature based on the reformer kinetic model used.

Additionally, this situation can be exacerbated by a condition in which the methanol flowing to the reformer leads (or lags) the methanol flowing into the burner to generate the required thermal energy for the steam reformation to occur. A shift could cause the burner temperature to be higher than that required by the reformer in a particular CSTR, jeopardizing reformer catalyst integrity, causing less methanol to be converted into hydrogen or more carbon monoxide to be generated.

3.2.2. Simulation setup

In this analysis, an arbitrarily selected 2 s lag in burner step input methanol flow was investigated. Preliminary results for a lag to a step response are discussed, and show that there appears to be minimal effect of a lag of 2 s. Several parameters were analyzed:

- Burner temperature
- Reformer temperature
- Reformer wall temperature
- Reformer MeOH
- Reformer CO
- Output H_2

The relative differences between the lag case and ideal case are small but more pronounced for the reformer MeOH,

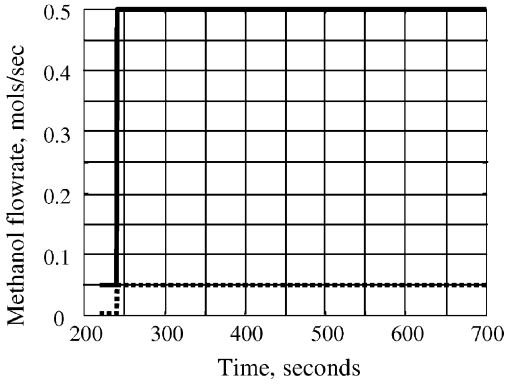

Fig. 16. Step input flowrate for sensitivity analysis. Reformer (—), burner (. . .).

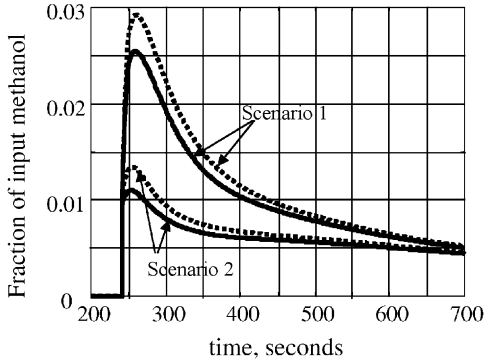

Fig. 18. Reformer exit MeOH—Scenarios 1 and 2; Scenario 2 is a more closely thermally integrated system than Scenario 1. Ideal condition (—), lagging condition (. . .).

CO and H_2 than the temperatures; therefore, only plots of the flows are shown.

In the step input analysis the flows are compared using three scenarios. Scenario 1 is the baseline for which $U_{\text{burner–wall–side}}A_{\text{wall}}$ and $U_{\text{reformer–wall–side}}A_{\text{wall}}$ are equal to 60 W/K per plate (for 100 plates). It was compared with two other scenarios in which the thermal coupling was enhanced. For Scenario 2, both *UA* values are 10 times the baseline. For Scenario 3, the *UA* values are the same as in Scenario 2; however, the wall mass is reduced 10-fold. As discussed in the step input section, the increased thermal coupling can improve overall methanol conversion. However, the lower thermal mass in Scenario 3 increases the sensitivity to the lag in burner input methanol.

In the model, the delay was introduced in the controller before the burner methanol input. Simulations were run with a 2 s input delay. Fig. 16 shows a snapshot in time of the methanol step input used for this analysis. The step input is preceded by an idle condition for 200 s. The reformer and burner flowrates reach a maximum of 0.5 and 0.05 mol/s, respectively.

3.2.3. Simulation results

The reformer exit unconverted methanol is shown in Fig. 17 versus time in seconds in response to the input shown in Fig. 16. The plot represents the unconverted methanol normalized by the input methanol. There is a slight increase in unconverted methanol in the lagging condition, which is an indication that fewer reactions are occurring in the reformer as a result of the lag in burner input methanol.

Furthermore, the initial spike in unconverted methanol for both conditions represents the maximum amount of methanol in the reactor at the time, which corresponds to the step up to the maximum input flowrate. The first-order response is due to the reformer thermal mass, which maintains a temperature at which activity can occur and methanol can be converted (note: the reformer methanol flow would not be a step response when used as a part of an overall system. It is used more as a diagnostic tool for this and other related studies).

An interesting point can be illustrated regarding the effect on exit methanol in a thermally integrated system. In further improving thermal integration by, for example, increasing the $U_{\text{burner–wall–side}}A_{\text{wall}}$ and $U_{\text{reformer–wall–side}}A_{\text{wall}}$ 10-fold, the effects of closer thermal coupling are more pronounced. Fig. 18 shows the effects of thermal integration on unconverted methanol, which decreases for the more closely thermally integrated system (Scenario 2).

Fig. 19 illustrates exit MeOH for Scenario 3 to be compared with Scenarios 1 and 2 in the previous figure.

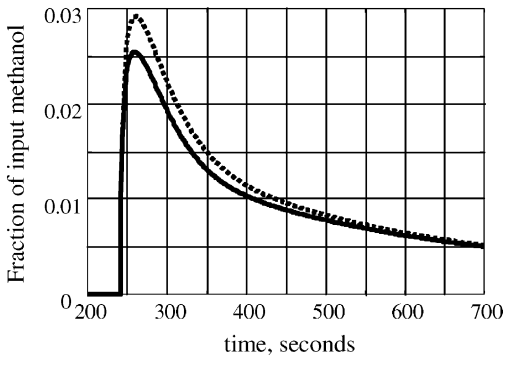

Fig. 17. Reformer exit MeOH—Scenario 1. Ideal condition (—), lagging condition (. . .).

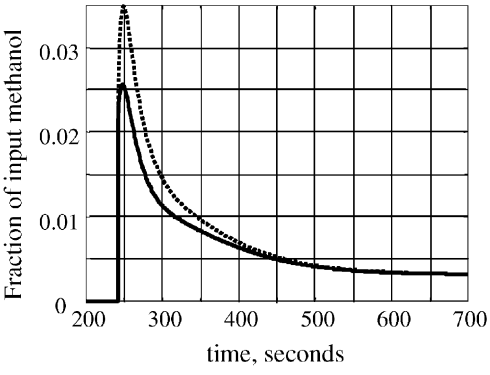

Fig. 19. Reformer exit MeOH—Scenario 3. Ideal condition (—), lagging condition (. . .).

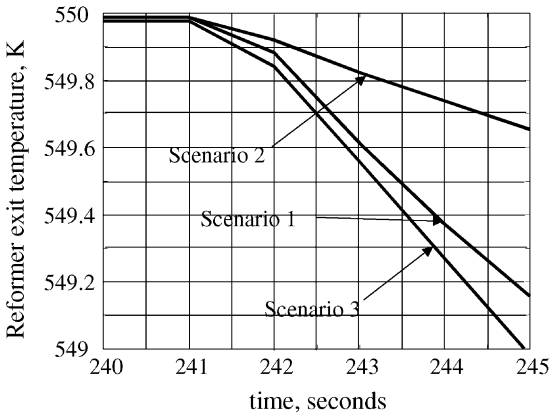

Fig. 20. Reformer exit temperature before and after step input.

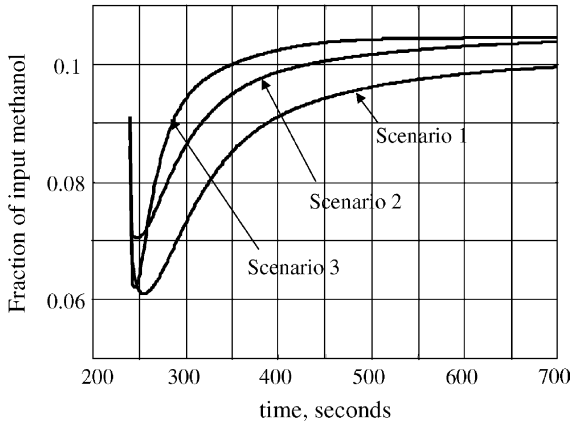

Fig. 22. Reformer exit CO—ideal condition.

Scenario 2 represents improved methanol conversion. The exit MeOH after the stepup for Scenario 3 exceeds that of Scenarios 1 and 2 due to reduced reaction rates resulting from lower exit temperatures. The spike in exit MeOH for all scenarios corresponds to a decrease in exit temperature after the step input as seen in Fig. 20. However, the lower mass in Scenario 3 has lower thermal energy and a greater drop in temperature after the methanol step input. Furthermore, the effect of lag on the decreased mass in Scenario 3 is twice that of Scenarios 1 and 2, indicating increased sensitivity to a delay in burner input methanol.Fig. 21 is the reformer exit hydrogen response to the methanol step input. There appears to be negligible affect of the lag condition on the hydrogen generated in the reformer, although it appears that slightly less hydrogen is produced in the lag condition. The drop in hydrogen corresponds to a drop in the conversion ratio since the input methanol is stepped up to the maximum level. During this period the thermal energy has yet to be transferred fully from the burner to the fuel in the reformer. For the remainder of the simulation the hydrogen responds to the maximum input methanol with first-order behavior.

Figs. 22 and 23 are the ideal and lag reformer exit carbon monoxide responses to the methanol step input. The lagging condition produces slightly *less* CO than the ideal condition since there are slightly less reactions to convert methanol to CO and hydrogen. This is consistent with the plots in Figs. 17 and 21 in which there is more unconverted methanol and less exit hydrogen for the lag condition. The CO drops with the step up in methanol flow and gradually reaches steady state for the remainder of the simulation.

Another point with respect to the CO response is worth mentioning. The methanol step input is preceded by an idle condition during which the methanol input flow is held constant for around 200 s and then decreases as shown in Fig. 24. This results in an upward spike in CO, shown in Fig. 25 for the ideal condition and Fig. 26 for the lag condition, since whatever MeOH that exists in the reactor converts to CO as the reformer temperature is high. This behavior is also seen in experiments conducted by [13].

The results presented have illustrated some effects of lag in burner input methanol on a limited set of fuel processor output parameters, such as unconverted methanol, exit hydrogen and exit CO. The results also highlight conditions that could exhibit sensitivity to lag such as reduced thermal mass. The results presented here have focused on a methodology to illustrate these effects by using a transient step

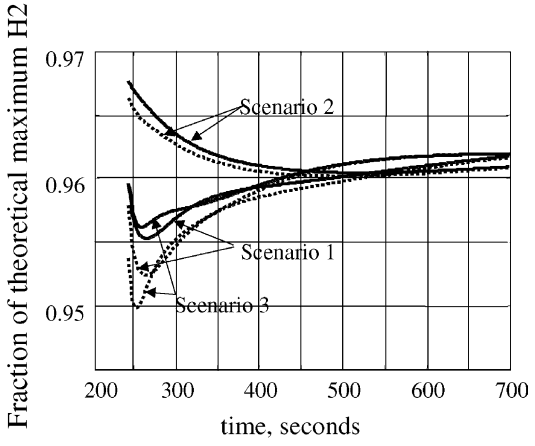

Fig. 21. Reformer exit H_2: ideal condition (—), lagging condition (. . .).

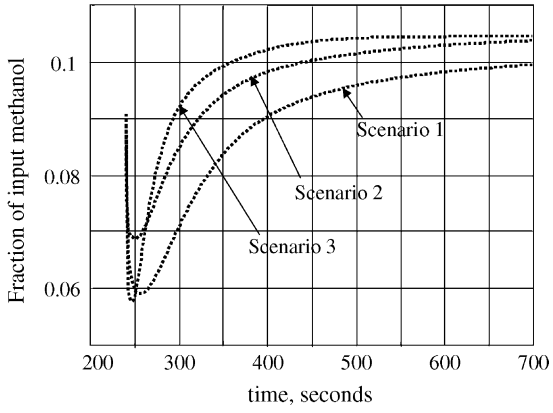

Fig. 23. Reformer exit CO—lagging condition.

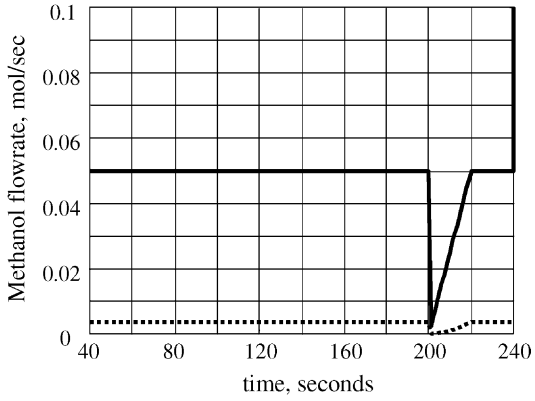

Fig. 24. Idle condition flowrate before step input: reformer (—), burner (. . .).

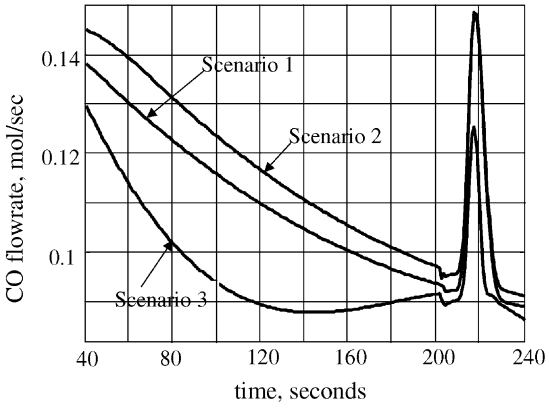

Fig. 25. CO response to drop in flowrate—ideal condition.

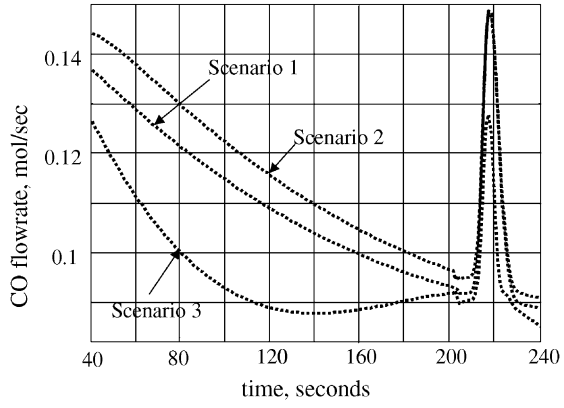

Fig. 26. CO response to drop in flowrate—lagging condition.

response. Preliminary results for a step input show that there appears to be minimal effect of a lag on the order of 2 s.

3.3. Dynamic impact

During dynamic operation of the fuel cell vehicle, the response of the fuel processor becomes critical and is very strongly influenced by the extent of thermal integration between the reformer and the burner. Fig. 27 shows exit

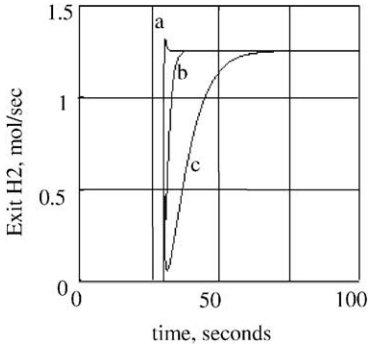

Fig. 27. Transient step response of the fuel processor. Decreasing levels of thermal integration (from case a to case c).

H_2 response to a step change in methanol flow from idle to 100% for burner/reformer systems with different thermal integration. Case (a) represents the case in which $U_{\text{burner–wall–side}}A_{\text{wall}}$ and $U_{\text{reformer–wall–side}}A_{\text{reformer}}$ are 60 W/K. Case (b) represents a case in which the *UA* values are an order of magnitude lower than case (a), and case (c) *UA* values are an order of magnitude lower than case (b). It can be seen that the dynamic response time for case (c) is around 50 s.

In case (c), there is poor conversion of methanol to hydrogen during the transient period. What actually happens is that due to poor thermal integration between the burner and the reformer, the thermal energy from the burner cannot be quickly transferred to the reformer. This results in a drop in the reformer catalyst temperature during the initial transient period and this in turn reduces the catalyst activity.

For case (a), representing the highest relative level of thermal integration, the result is a quicker dynamic response. In contrast to cases (b) and (c), the response time is 1–2 s. A point to note is that in addition to thermal integration, thermal mass can play a role as energy storage that maintains a temperature at which activity can occur and methanol can be converted.

The nature of the transient response also deserves some explanation. The initial response from the fuel processor seems instantaneous. This is because the reformer has a finite volume and the latter half of the fuel processor is rich in hydrogen. When the methanol/water mixture comes into the reformer, it effectively pushes the hydrogen-rich reformate out of the fuel processor (note that the reformer is operated in a constant pressure mode). However, this scenario cannot be sustained and the final rise in the conversion is due to the fact that the thermal energy transfer approaches the final steady state value. Note that steam generation and fuel vaporization have an impact on transient response; however, while these processes are important they have not been considered here.

3.4. Burner emissions

Two burner configurations have been studied: (a) adiabatic and (b) heat loss via thermal integration with the

reformer. For each configuration, temperature profiles and NO_x formation are compared. The catalytic burner simulation results forecast low NO_x emissions from the burner for case (b).

3.4.1. Thermal Integration effect on burner temperature

Fig. 28 shows the temperature profile of the adiabatic and thermally integrated cases, indicating a lower and more uniform temperature distribution in thermal integration.

3.4.2. NO_x emissions

It is well accepted [14–16] that there are three types of NO_x formation: thermal NO_x, prompt NO_x and fuel NO_x. Thermal NO_x is formed by the oxidation of nitrogen and is nearly linearly dependent on residence time and rises exponentially with temperature. Prompt NO_x occurs in reactions occurring under fuel rich conditions. Fuel NO_x results from the oxidation of nitrogen-containing compounds within the fuel. The following assumptions were made for the NO_x formation model:

(1) Methanol has no nitrogen-containing compounds [14] and the combustion mixture is lean (stoichiometric ratio = 1.5); therefore, only thermal NO_x, and not prompt or fuel NO_x, occurs. The prediction of the NO_x emission characteristics is made using a model in which NO_x formation occurs only in the gas.

(2) Of the dominant compounds considered under the category "NO_x," such as nitric oxide (NO), nitrogen dioxide (NO_2), and nitrous oxide (N_2O), NO comprises close to 95% of NO_x emissions in combustion processes [17]. Therefore, only NO emissions are modeled. The reactions equations that make up the Zeldovich mechanism [18] for NO formation are well accepted [14–17]:

$$O + N_2 \Leftrightarrow NO + N \quad (13)$$

$$N + O_2 \Leftrightarrow NO + O \quad (14)$$

$$0.5O_2 \Leftrightarrow O \quad (15)$$

The reaction rate expression and reaction rate and equilibrium constants are obtained from [17]. Deriving rate expressions for NO using the reaction Eqs. (13) and (14) and applying the steady state assumption for N yields the expression in Eq. (16). The subscripts for the reaction rate constants correspond to reaction Eqs. (13) and (14).

$$\frac{d[NO]}{dt} = \frac{2k_{13}[O][N_2]\{1 - ([NO]^2/K_{p,NO}[N_2][O_2])\}}{1 + (k_{-13}[NO]/k_{14}[O_2])} \quad (16)$$

Parameter values are as follows:

$$k_{13} = 1.4 \times 10^{14} e^{-315.5/\bar{R}T} \times 10^{-6},$$

$$k_{14} = 6.4 \times 10^{9} e^{-26.15/\bar{R}T} \times 10^{-6},$$

$$k_{-14} = 1.6 \times 10^{9} e^{-161.5/\bar{R}T} \times 10^{-6},$$

and

$$K_{13}K_{14} = \left(\frac{k_{13}}{k_{-13}}\right)\left(\frac{k_{14}}{k_{-14}}\right) = \frac{[NO]^2}{[N_2][O_2]} \equiv K_{p,NO}$$

Using these equations and values for $K_{p,NO}$ as provided in [17] for $N_2 + O_2 \Leftrightarrow 2NO$, k_{-13} can be solved. [O] in Eq. (15) is then determined using the expression $K_{p,O} = [O]_e(\bar{R}T)^{1/2}/[O_2]_e^{1/2}$ with the assumption that [O] may be set equal to $[O]_e$ (e: equilibrium) in the hot products for the reaction $0.5O2 \Leftrightarrow O$. Values for $K_{p,O}$ are found in the literature [19].

Fig. 29 shows the equilibrium NO concentration values calculated in the model using the above equations validated against the predicted equilibrium NO concentration values as published by [17]. Correlation between the model values and the published predictions is greater than 99% using the Pearson correlation method.

Fig. 30 shows the NO emissions for the adiabatic and thermally integrated cases. As Fig. 28 shows, even while gas adiabatic temperatures are over 1000 K, the emissions in Fig. 30 for the adiabatic case (a) with a step input of methanol are considerably lower than emissions formed at equilibrium at similar temperatures. As stated earlier, thermal NO_x is nearly linearly dependent on residence time and rises

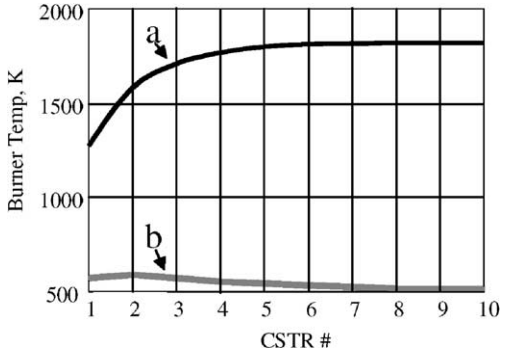

Fig. 28. Temperature along burner: (a) adiabatic case, (b) thermally integrated case.

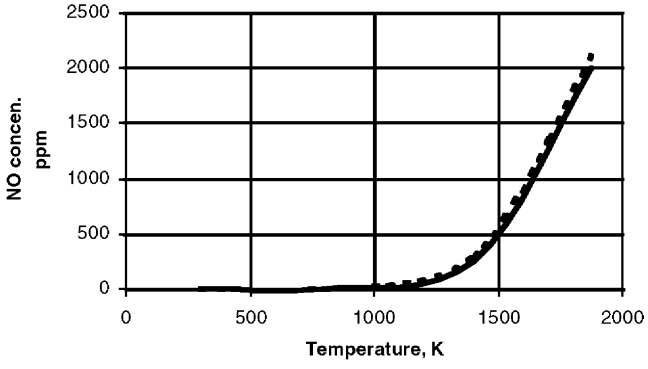

Fig. 29. Published values and model values for equilibrium NO concentration: (—) published values, (– – –) model values.

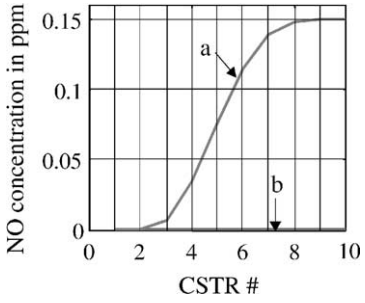

Fig. 30. NO emissions for adiabatic and thermally integrated cases: (a) adiabatic, (b) thermally integrated.

exponentially with temperature. A step input flowrate of methanol implies a flowrate of nitrogen and oxygen in the combustion products, or a finite residence time; therefore, *NO emissions are lower than in equilibrium in which nitrogen and oxygen molecules have effectively an infinite residence time*. This behavior is supported by [17], whose studies indicate that it is undesirable to maintain the reacting mixtures at high temperatures for long periods of time.

Thermal integration case (b) appears to have a significant impact on the level of NO emissions by lowering the burner temperature. Experimental results seem to support this observation; for example, the work by [5] using the plate configuration for methane combustion resulted in NO_x emissions below 1 ppm.

4. Conclusions

Section 2 described the steps by which a detailed model was developed for a thermally integrated burner/reformer system. Key results for Section 2 are listed below:

(1) The PFR/CSTR methodology was selected from the literature to build a numerical model that balanced accuracy with computation time.
(2) Results from simulations were analyzed to determine the importance of added complexity in the burner model and revealed that the simpler, less computationally intensive model, or the pseudo-homogeneous model, could be used in lieu of the heterogeneous model.
(3) Key parameters were made scalable while maintaining the validity of using the original reaction kinetics.

Section 3 described the simulation results that show the effects of thermal integration on: (a) reformer temperature and emissions especially when varying spatial parameters such as catalyst loading, (b) sensitivity to changes in input flow or thermal mass, (c) dynamic response, and (d) burner emissions. Key results for Section 3 are listed below:

(1) Varied catalyst loading can play a role in decreasing reformer temperature and CO emissions.
(2) For the parameters used in the sensitivity analysis, a two second lag in the step input of burner input methanol had a more pronounced (while still minimal overall) effect on plate configurations that had a higher heat transfer coefficient and lower thermal mass than the base case.
(3) Dynamic response can be greatly affected by thermal integration: a thermally well-integrated system can have an order of magnitude decrease in step response times.
(4) Reducing burner temperature through thermal integration can minimize burner emissions such as nitric oxide.

A final conclusion reached from this research is that the full impacts of thermal integration have yet to be explored and studied in the context of the fuel processor and the overall indirect methanol fuel cell system.

5. Future research

This work has focused on results from a fully warmed up, thermally integrated burner/reformer system using standard industrial catalysts. Further development on the fuel processor could focus on the following issues:

- Cold start: warm up time, emissions and fuel consumption.
- Different burner and reformer catalysts.
- Other variations in burner catalyst loading.
- Variations in reformer catalyst loading.
- Control strategies that affect the reformer's ability to provide the necessary hydrogen to the fuel cell stack.

Acknowledgements

We would like to acknowledge the hard work and contributions of the UC Davis Fuel Cell Vehicle Center modeling team members: Dr. Claudia Villa Diniz, Joshua Cunningham, Anthony Eggert, Parvastu Badrinarayanan, Dr. Jose Fernando Contadini, Dr. Karl-Heinz Hauer, David Friedman, Monterey Gardiner.

Appendix A. Validation of heterogeneous burner model

The heterogeneous burner model was based on the study by [8], and this study was selected for the following reasons. [8] conducted experimental and numerical analysis to evaluate the performance of a catalytic combustor with a methanol mixture. Other studies discuss transient analyses with methane, propane and other hydrocarbon–air mixtures. [8] was consulted for the present work because of the provision of surface and gas reaction rate constants for methanol combustion. Furthermore, [8] provides a detailed analysis of start-up emissions, which is not

considered in the present work but will be a reference for future work.

The prediction of the temperature profile is made using a heterogeneous model in which reactions occur both on the surface and in the gas. The following assumptions were made in the derivation of the energy and specie balance equations for the catalytic combustion of methanol:

(1) Radiation within the combustor and to the surroundings is neglected.
(2) Pressure drop is neglected.
(3) The heat loss from the combustor is assumed to be only to the reformer and not to the ambient environment.
(4) The gas mixture is an ideal gas.
(5) Intermediate reaction products, such as formaldehyde and carbon monoxide, are not considered. Complete conversion of methanol to carbon dioxide and water is assumed.

The modeling methodology uses the CSTR approach and energy and species balance calculations are performed in each CSTR. The surface energy balance is shown in Eq. (A.1).

$$\dot{E}_{\text{stored}} = \dot{E}_{\text{in}} - \dot{E}_{\text{out}}$$

$$\rho_{\text{cat}} C_{p_{\text{cat}}} S_{\text{cat}} A_c \Delta x^2 \frac{dT_{\text{cat}}}{dt} = S_{\text{cat}} A_c \lambda (T_{\text{cat}(x+1)} - 2T_{\text{cat}}(x) + T_{\text{cat}(x-1)}) + S_{\text{cat}} A_c \Delta x^2 \xi h_t \times (T_g - T_{\text{cat}}) + \left(\sum \left[\frac{dn_{i_{\text{cat}}}}{dt} h_i(T_{\text{cat}}) \right]_{\text{prod}} + \sum \left[\frac{dn_{i_{\text{cat}}}}{dt} h_i(T_g) \right]_{\text{reac}} \right) \Delta x - \dot{Q}_{\text{reformer}} \Delta x \quad \text{(A.1)}$$

Finite difference formulation is used for the heat conduction term, and enthalpy flow to and from the surface and gas is taken into account. With the exception of parameters described earlier, listed below are details of the parameters in Eq. (A.1).

- S_{cat} is the closed frontal area fraction (i.e. 1-S, where S is the open frontal area fraction of 0.64 [8].
- A_c is the reactor cross-sectional area, and Δx is the length of one CSTR.
- In the conduction term, λ is the gamma alumina thermal conductivity of 0.94 W/mK [8], $T_{\text{cat}(x)}$ is the catalyst temperature of one CSTR, $T_{\text{cat}(x+1)}$ is the catalyst temperature for the CSTR downstream of $T_{\text{cat}(x)}$ (recall that the plug flow reactor is represented by a series of 10 CSTRs), and $T_{\text{cat}(x-1)}$ is the catalyst temperature for the CSTR upstream of $T_{\text{cat}(x)}$.
- In the convection term, the specific surface area, ξ is 2700 m^2/m^3 [8], the heat transfer coefficient, h_t is 94 W/m^2 K [9] and T_g is the gas temperature.
- The third term on the right hand side of the equation represents heat flow of surface species arriving as reactants and leaving as products.

The gas energy balance is shown in Eq. (A.2).

$$\left(\sum n_i C_{p_i}\right) \frac{dT_g}{dt} = \sum F_{i(\text{in})} h_{i(\text{in})} - \sum \left(F_i + \frac{dn_{ig}}{dt} \right) h_i - A_c \Delta x \xi h_t (T_g - T_{\text{cat}}) - \left(\sum \left[\frac{dn_{i_{\text{cat}}}}{dt} h_i(T_{\text{cat}}) \right]_{\text{prod}} + \sum \left[\frac{dn_{i_{\text{cat}}}}{dt} h_i(T_g) \right]_{\text{reac}} \right) \quad \text{(A.2)}$$

The mass transfer coefficient, h_D, rate constants k_1 and k_2 and reaction and rate equations are the same as shown earlier in Eqs. (1)–(3). The species balance equations are the same as shown earlier in Eqs. (4)–(7). Only Eq. (8) differs slightly as shown in Eq. (A.3): instead of a single temperature T_{burner}, T_g is used, as the gas and surface temperatures are determined separately in the heterogeneous model.

$$F_T = \sum F_{i(\text{in})} - \sum (r_{i_g} + r_{i_{\text{cat}}}) + \frac{PV_{\text{void}}}{\bar{R} T_g^2} \frac{dT_g}{dt} \quad \text{(A.3)}$$

Note that calculations are done with moles and therefore use the universal gas constant $\bar{R}$; however, while moles are not conserved, mass is conserved. This condition was verified within the model. The initial condition for the surface and gas temperatures are $T_{\text{cat}} = T_g = 550$ K, where the surface and gas are assumed to be fully warmed up at time $t = 0$. The initial conditions for moles are $n_{O_2} = 0.2 n_T$, and $n_{N_2} = 0.8 n_T$ assuming only air exists within the burner at $t = 0$.

Fig. 31 shows a comparison of the [8] and this paper's model temperature profiles using parameters used in [8]—input temperature of 393 K, relative air/fuel ratio of 3.4, and space velocities of 3700, 5700, 8500 and 13000 h^{-1}. Space velocity (SV) is defined as the ratio of the feed volumetric flowrate at STP to the reactor volume. [8] provided no gas

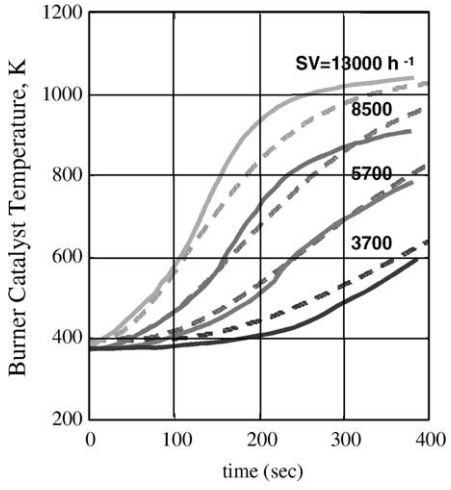

Fig. 31. Comparison of published and model temperature profiles. Relative air/fuel ratio = 3.4, inlet $T = 393$ K and space velocities (SV) are as indicated [8]. (—) [8], (– – –) this paper's model.

temperature profiles in this particular study so a comparison of the catalyst temperature is shown here.

Simulation results of the adiabatic case were compared with the experimental temperature profiles provided by [8] with a correlation of greater than 98% using the Pearson correlation method.

Appendix B. Discussion of *UA* parameter

The main parameter used in the models to thermally couple the burner and reformer is *UA*, where *U* is the heat transfer coefficient and *A* is the area. Specifically, *UA* is the product of the heat transfer coefficient between the burner catalyst and wall and wall area ($U_{\text{burner–wall–side}}A_{\text{wall}}$) and the product of the heat transfer coefficient between the wall and reformer catalyst and wall area ($U_{\text{reformer–wall–side}}A_{\text{wall}}$).

The best way to determine these *UA* values would be from microscale experiments. It might also be possible to estimate *UA* from geometrical and thermal properties provided the appropriate physical properties can be accurately determined. Alternatively, given a value for *UA*, the correct set of thermal properties can lead to initial geometry estimates.

Both methods require a set of heat transfer equations. To illustrate the parameters used in these equations, Fig. 32 shows one plate with burner and reformer catalyst.

Note the inclusion of the film resistance on the hot burner side and the film resistance on the cold reformer side. In the pseudo-homogeneous reactor, the warming of gases and the catalyst is taken into account, but the gas is in thermal equilibrium with the catalyst. Most of the reactions take place on the surface; therefore, most of the heat is generated by those surface reactions. However, if the gas thermal storage rate were significant relative to reaction heat rate, the barrier, or film resistance between the gas and catalyst would have to be taken into account, requiring a heterogeneous reactor. It was found that the gas thermal storage rate was not significant relative to the reaction heat rate in both the reformer and burner. This claim can be shown quantitatively from model results.

The thermal storage rate is calculated using $(\sum(\dot{n}_{\text{out}\,i} - \dot{n}_{\text{in}\,i})c_{\text{p}_i})\Delta T$, where the flowrates are the in and out flows of each CSTR for the *i*th specie, ΔT is the temperature difference of the input and output flows, and c_{p_i} is calculated for each specie at the average temperature. The reaction heat rate is calculated by using $(\dot{n}_{\text{CH}_3\text{OH}_{\text{in}}} - \dot{n}_{\text{CH}_3\text{OH}_{\text{out}}})\Delta H_R$, where the net methanol flowrates for each CSTR are multiplied by the reaction heat. The reaction heat for methanol oxidation is 640,800 J/mol and for methanol steam reformation is 50,000 J/mol. Table 1 shows the ratios of thermal storage rate to reaction heat rate for just the first CSTR, as it is the highest among the series of CSTRs for both burner and reformer.

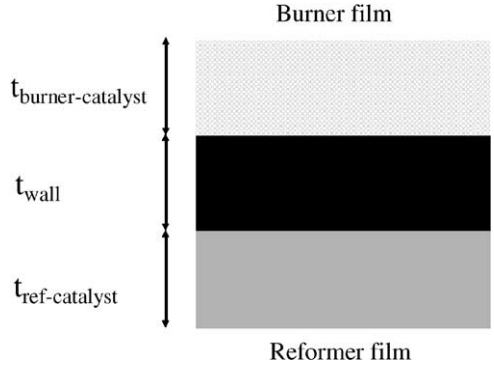

Fig. 32. Cross-section of plate with burner and reformer catalyst. Not to scale; *t* = thickness.

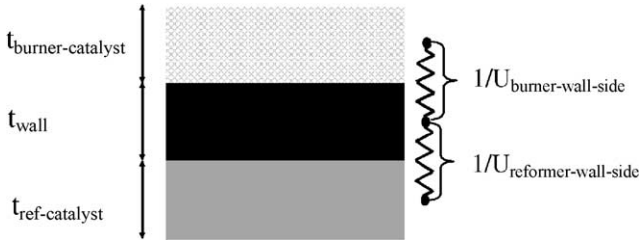

Fig. 33. Resistances across plate.

Table 1
Ratios of thermal storage rate to reaction heat rate

Regime	B (burner), R (reformer)	Thermal storage rate (J/s)	Reaction heat rate (J/s)	Ratio
Inlet—exit CSTR 1	B	1052	24435	0.043
	R	529	14419	0.037

As the results show, the ratio of thermal storage rate to reaction heat rate is negligible; therefore, it was decided to ignore the film resistances and consider only the burner catalyst, reformer catalyst and wall. The resistance to heat transfer by conduction is shown in Fig. 33. Note that the nodes defining the resistance boundaries are placed at the center of each section. This method was used in order to use the average temperature in the section, which was assumed to be in the center under steady state conditions.

B.1. Equations used

Fig. 34 provides the context by which the equations were derived.

The parameters *k* and *t* are the thermal conductivities and material thickness, respectively. An arbitrary, decreasing

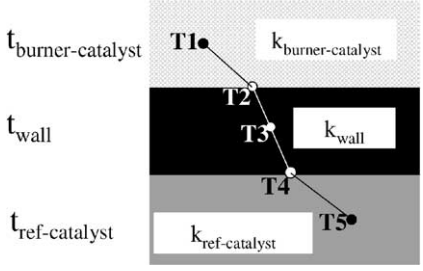

Fig. 34. Diagram for derivation of heat transfer equations.

temperature profile is assumed, represented by $T1$, $T2$, $T3$, $T4$ and $T5$. At steady state, the heat flux, q'', is identical in each section and can be described by the following equations. For the burner–wall–side:

$$\text{general equation}: \quad q'' = U\Delta T$$

$$q'' = \frac{k_{\text{burner-catalyst}}}{t_{\text{burner-catalyst}}/2}(T1 - T2)$$

$$\text{or} \quad q''\frac{t_{\text{burner-catalyst}}/2}{k_{\text{burner-catalyst}}} = T1 - T2 \tag{B.1}$$

$$q'' = \frac{k_{\text{wall}}}{t_{\text{wall}}/2}(T2 - T3)$$

$$\text{or} \quad q''\frac{t_{\text{wall}}/2}{k_{\text{wall}}} = T2 - T3 \tag{B.2}$$

Adding heat flux Eqs. (B.1) and (B.2) together, U is determined as shown in Eq. (B.3).

$$q'\left(\frac{t_{\text{burner-catalyst}}/2}{k_{\text{burner-catalyst}}} + \frac{t_{\text{wall}}/2}{k_{\text{wall}}}\right) = T1 - T3$$

$$U = \frac{k_{\text{burner-catalyst}}k_{\text{wall}}}{(t_{\text{wall}}/2)k_{\text{burner-catalyst}} + (t_{\text{burner-catalyst}}/2)k_{\text{wall}}} \tag{B.3}$$

A similar analysis can be made on the reformer-wall side. The full UA equations are shown in Eqs. (B.4) and (B.5).

$$U_{\text{burner-wall-side}}A_{\text{wall}} = \frac{k_{\text{wall}}k_{\text{burner-catalyst}}(V_{\text{burner-catalyst}}/Nt_{\text{burner-catalyst}})}{(t_{\text{wall}}/2)k_{\text{burner-catalyst}} + (t_{\text{burner-catalyst}}/2)k_{\text{wall}}} \tag{B.4}$$

$$U_{\text{reformer-wall-side}}A_{\text{wall}} = \frac{k_{\text{wall}}k_{\text{reformer-catalyst}}(V_{\text{reformer-catalyst}}/Nt_{\text{reformer-catalyst}})}{(t_{\text{wall}}/2)k_{\text{reformer-catalyst}} + (t_{\text{reformer-catalyst}}/2)k_{\text{wall}}} \tag{B.5}$$

The terms V_b/Nt_b and V_r/Nt_r, where V is volume and N is number of plates, represent per plate areas of the burner and reformer, respectively and are assumed to be equal in the plate configuration. Another area term, V_w/Nt_w could be used in lieu of either of the other two terms, as they are all equal, and given the assumption that the heat transfer area is the same as the physical area.

In the initial part of the analysis, the values for UA were selected using the work done earlier by [7]. The study by [7] on a shell and tube reformer/burner configuration illustrated the need for substantially higher heat transfer coefficients to achieve exit H_2 response, from 10 to 90%, of the order of 2 s, which is the response time required by the fuel cell system specifications used [11]. Therefore, the initial studies of the thermally integrated reformer/burner system were based on an assumption of setting both $U_{\text{burner-wall-side}}A_{\text{wall}}$ and $U_{\text{reformer-wall-side}}A_{\text{wall}}$ equal to 60 W/K per plate (for 100 plates), which is an order of magnitude higher than the values studied by [7].

Table 2
Material thermal conductivities

Plate section	Material	Thermal conductivity (W/m K)
Burner	γ Alumina [8]	0.94 [8]
Wall [20]	Stainless steel 316	14
	Plain carbon steel	60
	Al alloy 2024-T6	177
Reformer	Cu/ZnO/Al2O3 [12]	15 [21–23]

If the values of UA are estimated from the bulk material properties of the reformer and burner catalysts along with three different wall materials (Table 2), it was found that $U_{\text{burner-wall-side}}A_{\text{wall}}$ is up to an order of magnitude larger than $U_{\text{reformer-wall-side}}A_{\text{wall}}$, a direct effect of the much smaller burner catalyst mass (6 kg burner versus 30 kg reformer). However, it is unclear whether the properties of the burner catalyst will be valid for a coated, monolith geometry where the thermal path length and cross-sectional areas (when accounting for the voids) may be different, again indicating the need for laboratory studies for determining thermal properties of these materials.

Given that published experimental data about UA values for integrated burner/reformer systems is scarce, as a first step Eqs. (B.4) and (B.5) can be used to determine the initial estimates for additional simulations.

References

[1] H.K. Geyer, R.K. Ahluwalia, R. Kumar, in: Proceedings of the 31st IECEC on Dynamic Response of Steam-Reformed, Methanol-Fueled, Polymer Electrolyte Fuel Cell Systems, Washington, DC, USA, vol. 2, 1996, pp. 1101–1106.

[2] G.L. Ohl, J.L. Stein, G.E. Smith, Fundamental factors in the design of a fast-responding methanol-to-hydrogen steam reformer for transportation applications, Trans. ASME 118 (1996) 112–119.

[3] B. Emonts et al., Fuel cell drive system with hydrogen generation in test, J. Power Sources 86 (2000) 228–236.

[4] R.A.J. Dams, P.R. Hayter, S.C. Moore, The development and evaluation of compact, fast response integrated methanol reforming fuel processor systems for PEMFC electric vehicles, SAE Paper No. 2000-01-0010.

[5] van Driel, Marinus, Meijer, Marianne, A Novel Compact Steam Reformer for Fuel Cells, with Heat Generation by Catalytic Combustion Augmented by Induction Heating, 1998 Fuel Cell Seminar, Palm Springs, CA, 1998.

[6] J. Cunha, J.L.T. Azevedo, Modeling the integration of a compact plate steam reformer in a fuel cell system, J. Power Sources 86 (2000) 515–522.

[7] G.L. Ohl, Dynamic analysis of a methanol to hydrogen steam reformer for transportation application, Ph.D. dissertation, University of Michigan, 1995.

[8] K. Ito, B.C. Choi, O. Fujita, The start-up characteristics of a catalytic combustor using a methanol mixture, JSME Int. J., Ser. II 33 (4) (1990) 778–784.

[9] R.D. Hawthorn, Afterburner catalysts-effects of heat and mass transfer between gas and catalyst surface, AIChE Symp. Ser. 70 (137) (1974) 428–438.

[10] D.J. Worth, A. Spence, P.I. Crumpton, S.T. Kolaczkowski, Radiative exchange between square parallel channels in a concentric monolith structure, Int. J. Heat Mass Transfer 39 (7) (1996) 1463–1474.
[11] S. Chalk, Progress Report for Fuel Cell Power Systems, US DOE, October 2000.
[12] J.C. Amphlett, Hydrogen Production by Steam Reforming of Methanol for Polymer Electrolyte Fuel Cells, J. Hydrogen Energy 19 (2) (1994) 131–137.
[13] C.D. Dudfield, R. Chen, P.L. Adcock, A compact CO selective oxidation reactor for solid polymer fuel cell powered vehicle application, J. Power Sources 86 (2000) 214–222.
[14] Z.R. Ismagilov, M.A. Kerzhentsev, Catalytic fuel combustion—a way of reducing emission of nitrogen oxides, Catal. Rev. Sci. Eng. 32 (1/2) (1990) 51–103.
[15] A. Cybulski, J.A.Moulijn (Eds.), Structured Catalysts and Reactors, Marcel-Dekker, New York, 1998, p. 151.
[16] I. Glassman, Combustion, 1st ed., Academic Press, New York, 1977, pp. 210–223.
[17] K. Wark, C.T. Warner, Air Pollution, Harper and Row, New York, 1981, pp. 376–384.
[18] J. Zeldovich, The oxidation of nitrogen in combustion and explosions, Acta Physicochim. URSS 21 (1946) 577–628.
[19] R.D. Lide (Ed.), CRC Handbook of Chemistry and Physics, CRC Press, Boca Raton, 1999, pp. 5–81, 5–82.
[20] P.F. Incropera, D.P. De Witt, Fundamentals of Heat and Mass Transfer, 3rd ed., Wiley, New York, 1990.
[21] R.J. Farrauto, C.H. Bartholomew, Fundamentals of Industrial Catalytic Processes, Blackie Academic and Professional, London, New York, 1997, p. 376.
[22] D.R. Lide (Ed.), CRC Handbook of Chemistry and Physics, 81st ed., CRC Press, Boca Raton, 2000–2001, pp. 12–202,12–205.
[23] M.B. Bever (Ed.), Encyclopedia of Materials Science and Engineering, vol. 2, Pergamon Press, Oxford, 1986, p. 854.